Spectrochimica Acta Part A: Molecular and Biomolecular Spectroscopy 338 (2025) 126203

Contents lists available at ScienceDirect

Spectrochimica Acta Part A: Molecular and Biomolecular Spectroscopy

journal homepage: www.journals.elsevier.com/spectrochimica-acta-part-a-molecular-and-biomolecular-spectroscopy

Sensing of cyanide ion by tweaking the proton transfer

Mongoli Brahma [a], Arup Das Kanungo [a], Minati Das [a], Sam P. Mathew [b], Bithiah Grace Jaganathan [b], G. Krishnamoorthy [a,*]

[a] *Department of Chemistry, Indian Institute of Technology Guwahati, Guwahati 781039, India*
[b] *Department of Biosciences and Bioengineering, Indian Institute of Technology Guwahati, Guwahati 781039, India*

HIGHLIGHTS

- Selective CN$^-$ sensing was achieved in acetonitrile–water with LOD of 0.7 μM.
- Using surfactant, the LOD was improved to 0.2 μM.
- CN$^-$ breaks the intramolecular hydrogen bond, thereby averts the ESIPT.
- Addition of CN$^-$ triggers intermolecular proton transfer to led anion emission.
- Applied in water samples analysis, MDA-MB-231 cells imaging and logic gate.

GRAPHICAL ABSTRACT

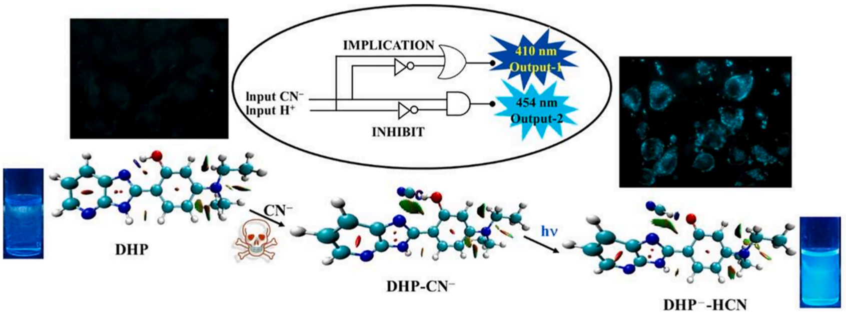

ARTICLE INFO

Keywords:
Fluorometric sensing
DFT
Water sample
Test strip
Cell imaging
Logic gate

ABSTRACT

The highly efficient sensing of cyanide ion was attained using a chemosensor, 2-(4′-diethylamino-2′-hydroxyphenyl)-1*H*-imidazo-[4,5-b]pyridine (DHP) by tuning its excited state intramolecular proton transfer to intermolecular proton transfer. Cyanide ion turns the weak blue emission of the chemosensor to bright cyan luminescence. The fluorescence is enhanced by 16 times in the presence of cyanide ion. The detection limit of CN$^-$ ion by DHP is 0.02 μM in acetonitrile. It is reversible, and the reusability was also tested for several cycles. A molecular logic gate was also constructed. The chemosensing was further tweaked by the medium. In addition, DHP has been practically applied for cyanide detection using paper strips, different water samples and sensing and imaging of cyanide ion in MDA-MB 231 breast cancer cells. To substantiate the mechanism of sensing ^{1}H-NMR titration, density functional theory (DFT) and time dependent density functional theory (TD-DFT) calculations were employed. The transition state structures and visualization of non-covalent interactions (NCI) from reduced density gradient (RDG) and scatter plots support the proposed mechanism.

1. Introduction

Cyanide is a vital anion in the production industries, including the manufacture of synthetic fibers, acrylics plastics, in metallurgy for electroplating, metal cleaning, gold mining, etc. [1,2,3]. Its' growing use in industries without proper handling and disposal, releases residual cyanide in environments including soil, rivers, etc. is lethal to humans [4]. Acute cyanide exposure causes serious health problems due to its

---

* Corresponding author.
E-mail address: gkrishna@iitg.ac.in (G. Krishnamoorthy).

https://doi.org/10.1016/j.saa.2025.126203
Received 22 February 2025; Received in revised form 26 March 2025; Accepted 7 April 2025

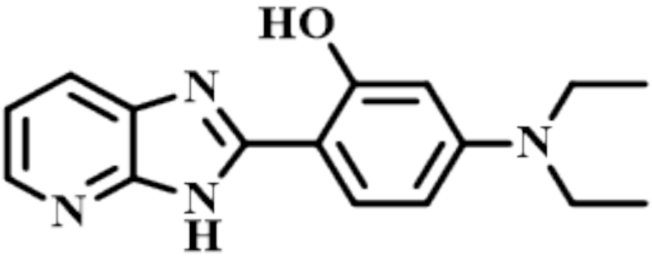

Chart 1. Structure of DHP.

ability to inhibit oxygen supply and electron transport through strong binding interaction with iron of heme units [5,6]. Cyanide was used as a chemical warfare agent by terrorists for mass destruction [7]. Studies also reported the presence of 23–26 μM cyanide in the fire victims' blood [8,9]. The cyanide permissible limit by World Health Organization (WHO) in drinking water is 1.9 μM [10,11]. Therefore, detection of cyanide is decisive. Among various methods for sensing critical analytes, fluorescent techniques proved to be effective with low cost synthesis, high sensitivity, easy to operate and in bio-imaging applications [12,13,14,15,16]. Many fluorescent probes with single-emission and dual emission have been explored. Among them, turn on-type fluorescent signals are preferable over turn off type fluorescent signals avoiding signal loss, improving detection sensitivity [17,18,19]. Furthermore, in the ratiometric method, the ratio of fluorescence intensities at different wavelengths was measured [20,21,22,23,24].

Solubility is a major concern for the fluorescent probes in pure aqueous medium. It can, however, be addressed by using different solvent systems or organic-aqueous mixtures [25,26,27]. Binding interactions in such systems are highly dependent on the microenvironment of molecule [28]. Several surfactant-assisted fluorescent amplification methods for the aqueous samples have been reported [29,30,31]. Surfactant at critical concentration forms aggregates called micelle, which are composed of a nanosized hydrophobic core, which can confine different organic molecules in their core. This helps in restoring photophysical properties of fluorescent probes, thereby boosting the response [32]. The mode of interactions by these probes mainly involves hydrogen-bonding interactions or nucleophilic reaction [33,34]. Various fluorescent probes for cyanide have been designed based on intramolecular charge transfer (ICT), Förster resonance energy transfer (FRET), aggregation-induced emission enhancement (AIEE) etc. [35,36,37]. Only a few probes have been reported based on excited state intramolecular proton transfer (ESIPT) process [38,39]. ESIPT based probes commonly possess an intramolecular hydrogen bond between a hydrogen bonding donor (–OH, $–NH_2$, etc.) and an acceptor (=N–, C=O, etc.) in close proximity. Upon light excitation, increase in the acidity of the donor and the basicity of the acceptor unit, which are in hydrogen bonding, changes, causing a cyclic photo-tautomerization. This results in tautomer emission with a characteristic large stoke shifted optical response [40,41]. Different ESIPT based scaffolds have been utilised for cyanide sensing. Zhu et al. developed chromene based chromogenic and fluorogenic probes which turn on ESIPT, giving tautomer emission at lower concentration of cyanide and at excess cyanide concentration –NH deprotonation dominates [21]. Rao et al. utilised a pyridine-hydrazone based ESIPT probe for colorimetric cyanide recognition due to –NH based deprotonation mechanism [13]. Liang et al. developed a Schiff based fluorescent light up cyanide sensor [38]. Zali-Boeini et al. developed a donor-π-acceptor system for cyanide sensing in which the cyanide ion turns off the ICT fluorescence [42].

In this work, a comprehensive approach to improve the selectivity and sensitivity of cyanide detection was investigated in different media, along with a deep insight into the mechanistic pathways of sensing, associated in the ground as well as in the excited state. The probe 2-(4′-diethylamino-2′-hydroxyphenyl)-1*H*-imidazo-[4,5-b]pyridine (DHP, Chart 1) emits normal and tautomer emissions at 410 nm at 470 nm, respectively in acetonitrile due to ESIPT [43]. Addition of cyanide, disrupts ESIPT, giving a light up fluorescence turn on anion emission. The mechanism was confirmed by ^{1}H NMR titration, reversibility study and DFT calculations.

2. Materials, methods and instruments

Tetrabutylammonium/sodium salts of CN^-, I^-, Br^-, F^-, OAc^-, ClO_4^-, Cl^-, HSO_4^-, SCN^-, NO_3^-, SO_3^{2-}, cetyltrimethylammonium bromide (CTAB) and trifluoro acetic acid (TFA) were obtained from Sigma Aldrich. HPLC grade solvents were procured from Spectrochem, India. DHP synthesis is reported elsewhere [43]. ^{1}H NMR and ^{13}C NMR was recorded in 400 MHz Bruker Instrument in dimethylsulfoxide-d_6 (Supplementary Material, Figs. S1 and S2). The UV–visible and steady state fluorescence measurements were carried out with 3 μM of fluorophore in acetonitrile and 5 μM of fluorophore in acetonitrile–water mixture and CTAB solution.

The absorption and the steady state emission spectra were recorded on Cary UV–visible spectrometer and HORIBA Jobin Yvon Fluoromax+ spectrofluorimeter, respectively. The fluorescence decays were recorded on Edinburgh Instrument Life-Spec-II of response time 50 ps and Hamamatsu microchannel plate as detector. Laser diode of 375 nm pulse width of 90 ps was used as the excitation source. Decay analysis were carried out by reconvolution method using FAST software provided by Edinburgh Instruments Ltd with goodness of fit value (χ^2). Zeiss Axio Observer fluorescence inverted was used for imaging.

DFT and TDDFT calculations were performed in Gaussian 16 program and the input files were created using Gauss View 6.0 [44,45]. The ground state and excited state structures were optimized using DFT and TDDFT, respectively using basis set 6-311++G(d,p) with Becke's three parameter exchange functional accompanying the Lee-Yang-Parr nonlocal correlation functional (B3LYP) [46,47,48]. Integral equation formalism polarizable continuum (IEF-PCM) model was used to perform calculation in acetonitrile [49]. The optimized geometries were confirmed with the absence of imaginary frequencies except in case of transition state. Potential energy curves (PEC) were constructed varying bond length along the possible proton transfer coordinates in the ground and excited states. The transition state for the proton transfer process that connects both species was identified and optimized by using the synchronous transit-guided quasi- Newton QST2 method [50].

The fluorescence yield and quantum yield of the samples were determined in reference to a standard solution (1 N Quinine sulfate of quantum yield 0.55) using the following equation:

$$\Phi_{\mathrm{S}} = \Phi_{\mathrm{R}}\frac{n_S^2}{n_R^2} \times \frac{A_R}{A_S} \times \frac{F_S}{F_R}$$

Here, *n*, *A* and *F* denotes the refractive index of the solvent, absorbance at the excitation wavelength and area under the emission spectra, respectively. The subscripts S and R refer to the sample and the reference, respectively. For quantum yield measurement, the emission spectra were recorded at wavelength 350 nm.

The limit of detection (LOD) was determined based on the fluorescence titration method [51]. LOD was calculated using the equation,

$$\mathrm{LOD} = 3\sigma/\mathrm{k}$$

Where, σ is the standard deviation of 5 blank measurements; k is the slope obtained from concentration versus intensity plot.

The binding constants of DHP for different analytes are determined using the following Benesi-Hildebrand equation [52].

$$\frac{1}{I - I_0} = \frac{1}{K_a(I_{max} - I_0)[C]^n} + \frac{1}{I_{max} - I_0}$$

where I_0, I, and $I_{\max}$ are the emission intensities of the probe in the absence of analyte, at an intermediate analyte concentration, and at a concentration of complete interaction with analyte, respectively. K_a is the binding constant, C is the concentration of analyte, and n is the

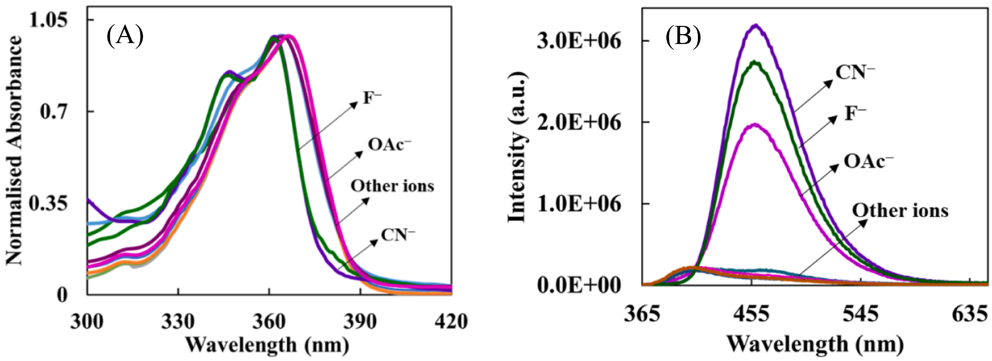

Fig. 1. (A) Normalised absorption spectra and (B) emission spectra (λ_{exc} = 350 nm) of DHP in presence of anions (1 mM) CN^-, I^-, Br^-, F^-, OAc^-, ClO_4^-, Cl^-, HSO_4^-, SCN^-, NO_3^-, SO_3^{2-} in acetonitrile.

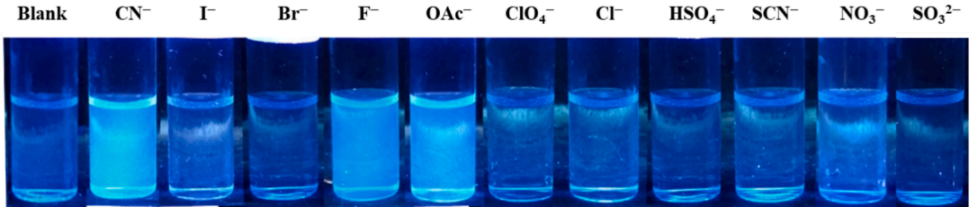

Fig. 2. Under 365 nm UV light illumination, fluorescence color change of DHP with different anions (from left to right: (1 mM) Blank, CN^-, I^-, Br^-, F^-, OAc^-, ClO_4^-, Cl^-, HSO_4^-, SCN^-, NO_3^-, SO_3^{2-}) in acetonitrile.

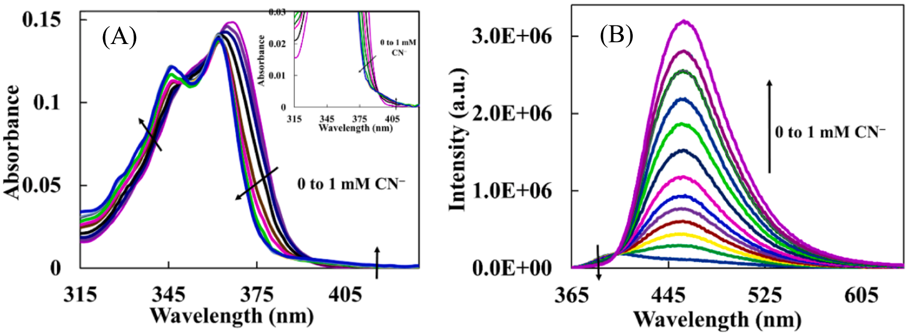

Fig. 3. (A) Absorption spectra and (B) emission spectra (λ_{exc} = 350 nm) of DHP with increasing concentration of CN^- (0–1 mM) in acetonitrile.

number of analytes bound per probe molecule.

Reduced density gradient (RDG) scatter plots and RDG isosurfaces are generated through Multiwfn [53], and VMD software [54], respectively. The x- and y- coordinates are represented below.

$$\Omega = \mathrm{sign}(\lambda_2)\,\rho$$

$$\mathrm{RDG} = \frac{1}{2(3\pi^2)^{1/3}}\frac{|\nabla\rho|}{\rho^{4/3}}$$

The strength of non covalent interaction (NCI) interaction is measured as a product of electron density $\rho(r)$ and sign of the second-lowest eigenvalues of electron density hessian matrix (λ_2).

3. Results and discussion

3.1. *Sensing of cyanide ion in acetonitrile*

The absorption and fluorescence response of DHP toward different anions (1 mM) CN^-, I^-, Br^-, F^-, OAc^-, ClO_4^-, Cl^-, HSO_4^-, SCN^-, NO_3^-, SO_3^{2-} were examined in acetonitrile (Fig. 1). DHP absorbs at 367 nm with a shoulder at 351 nm. In presence of CN^- and F^-, the absorption band is shifted to 360 nm along with the shoulder which is shifted to 347 nm (Fig. 1A). Other anions have negligible effect on the absorption spectra. DHP emits normal emission in 410 nm and tautomer at 470 nm [43], in presence of CN^-, F^- and OAc^-, a new emission band was observed at 454 nm, whereas other anions do not produce much changes (Fig. 1B). The fluorescence intensity of the new emission in presence of CN^-, F^- and OAc^-, is substantially enhanced in comparison to the blue emission in the absence of these anions. Under UV illumination, a clear naked eye colour change from blue to cyan was observed in presence of CN^-, F^- and OAc^- (Fig. 2). The enhancement in fluorescence in presence of cyanide ion is 16 times higher than in the absence of cyanide ion.

To understand the mechanism of sensing and fluorescence enhancement, the absorption and fluorescence spectra were recorded at different concentrations of cyanide ion (Fig. 3(A and B)). The absorption band at 367 nm and shoulder at 351 nm of DHP were slowly blue shifted with an increase in concentration. As stated earlier, upon addition of CN^- the normal emission is red shifted from 410 nm band to 454 nm with a huge increase in fluorescence. The total fluorescence yield (normal + tautomer emission) of DHP in the absence of cyanide is 0.03.

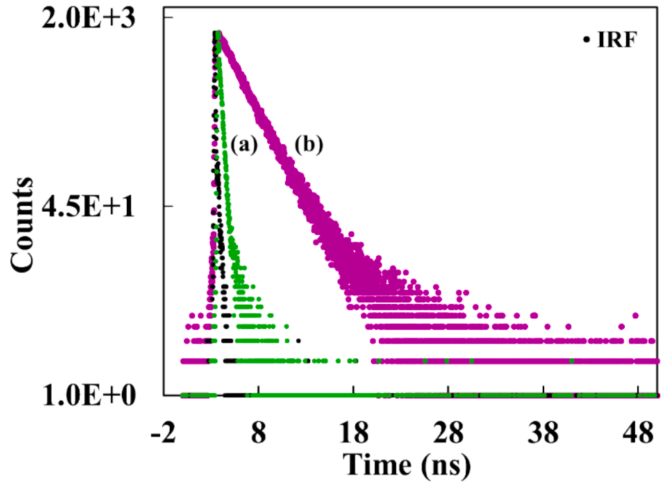

Fig. 4. The fluorescence decay of DHP (a) monitored at 410 nm in the absence and (b) monitored at 454 nm in presence of CN^- (1 mM) in acetonitrile, $\lambda_{exc} = 375$ nm.

Table 1
Absorption maximum (λ^{ab}_{max}, nm), emission maximum (λ^{fl}_{max}, nm) and fluorescence lifetime (τ, ns) of DHP in absence and presence of CN^- and the χ^2 value for the decay fit.

	$\lambda^{ab}_{(max)}$	$\lambda^{fl}_{(max)}$		τ^{a} (ns)	χ^2
		Shorter wavelength	**Longer wavelength**		
DHP	351, 367	410	470	**Monitored at 410 nm** 0.2 (87 %)[a] 1.3 (13 %)[a]	
DHP-CN^-	347, 360, 405	454	–	**Monitored at 454 nm**2.6 (100 %)[a]	

[a] The relative amplitude are given in parenthesis. The error in the fluorescence lifetime is ± 0.1 ns.

The fluorescence quantum yield of DHP in the presence of cyanide is 0.50. The new emission band is blue shifted with respect to tautomer emission. This behaviour is characteristic of anion emission [55]. When enol 'OH' proton is deprotonated to form an anion, it will increase the conjugation within the molecule, which results in red shifted emission compared to normal emission. The absorption spectrum of the anion is also red shifted with respect to enol absorption [55]. But the addition of cyanide resulted in blue shift. Though a long red tail is observed upon addition of cyanide, it is very weak, suggesting negligible amount of formation of anion. However, such a blue shift is consistent with the breaking of intramolecular hydrogen bond. Cyanide ion broke the intramolecular hydrogen bond by forming an intermolecular hydrogen bond. The formation of such DHP-CN^- complex is confirmed by mass spectrometry (ESI-MS analysis (Fig. S3), [DHP-CN^-] [*m/z:* 309.1738; calculated: 309.1584]). Upon photoexcitation, due to an increase in acidity of the phenolic proton, the intermolecular proton transfer occurs from DHP to the cyanide ion, that resulted in anion. The formation of anion led to red shift in the emission spectra along with an incredible increase in fluorescence. Further, the Job plot (Fig. S4A) also accounts for the 1:1 association of DHP-CN^- and the association constant was determined to be 1.5×10^4 M^{-1} from Benesi-Hildebrand plot, with a linear fit, correlation factor $r^2 > 0.99$ (Fig. S4B). The fluorescence emission was biexponential in the absence of cyanide ion (Fig. 4 and Table 1) due to normal and tautomer emission. In the presence of cyanide ion, DHP emits single fluorescence due to anion formation (Fig. 4 and Table 1). The breaking of the intramolecular hydrogen bond prevented the tautomer formation. The LOD for sensing of cyanide is 0.02 μM (Fig. S5).

Further, to substantiate the mechanism, the NMR spectra of DHP were recorded in dimethylsulfoxide-d_6 (Fig. 5). The peak of 'OH' proton of DHP appears at 12.93 ppm and it disappears in the presence of one equivalent of cyanide ion indicating the strong interaction of cyanide with 'OH' proton. The other aromatic protons peaks also shift from 8.2–6.2 ppm to 8.1–6.1 ppm, because the interaction led to an increase in electron density, resulting in the shielding of the corresponding protons.

Optical reversibility is an important aspect for the possible re-use of the probe. Protonation of DHP-CN^- was carried out by adding TFA. Addition of TFA reverts the spectrum to the original. The experimental reproducibility of CN^- recognition by DHP is shown in Fig. 6. 5 cyclic additions of CN^-, followed by TFA addition were performed. This led to colour change of the solutions from blue to cyan, and back to blue again (Fig. 6A inset). Further, this experiment also suggests that existence of anion emission which was turned off by TFA addition due to protonation of anion to form neutral DHP.

Also, bar diagram (Fig. 7) was constructed at emission maximum 454 nm. The interference and anti interference studies suggested DHP has strong sensing ability for CN^- followed by F^- and OAc^-, because of this selective recognition for cyanide may be affected. Therefore, further

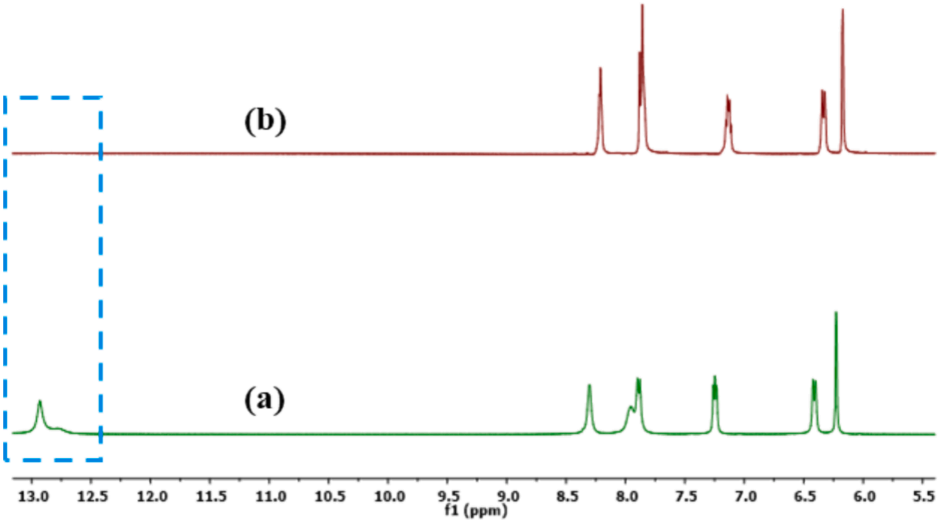

Fig. 5. ^{1}H NMR spectra of DHP in (a) the absence and (b) the presence of 1 equivalent of CN^- in DMSO-d_6.

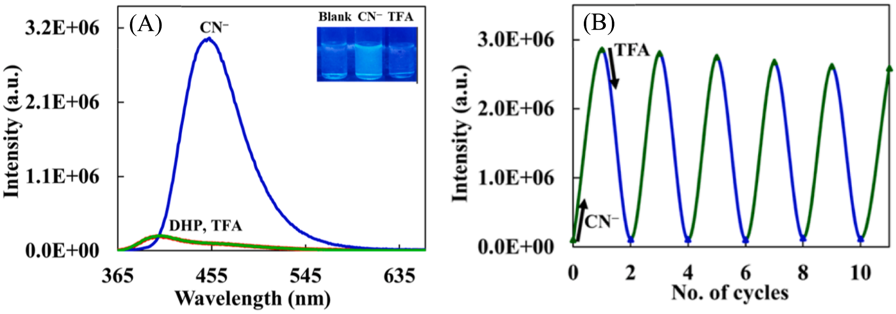

Fig. 6. (A) Emission spectra of DHP in absence and presence of cyanide and then further addition of TFA. Inset shows the colour change upon addition of CN^- and then TFA under UV illumination at 365 nm. (B) Intensity (at 454 nm) versus no. of repeated cycles plot obtained: DHP upon addition of CN^- (1 mM) and then with TFA (0.9 mM) in acetonitrile, λ_{exc} = 350 nm.

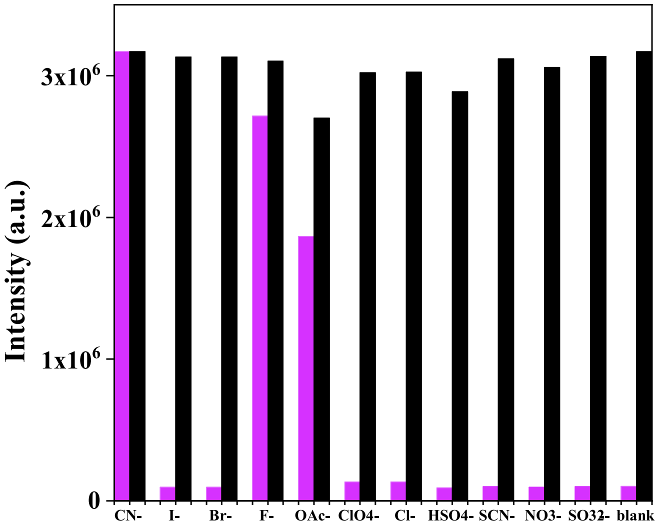

Fig. 7. Interference bar diagram at emission wavelength 454 nm: purple bar represents DHP in presence of (1 mM) anions (1) CN^-, (2) I^-, (3) Br^-, (4) F^-, (5) OAc^-, (6) ClO_4^-, (7) Cl^-, (8) HSO_4^-, (9) SCN^-, (10) NO_3^-, (11) SO_3^{2-} (12) blank and black bar represents addition of cyanide to the respective anions (λ_{exc} = 350 nm).

experiments were carried out to improve the selectivity of cyanide recognition by probe DHP.

3.2. Controlling the ion sensing by medium

The interaction of the anion with solvent shall reduce the interaction of the anion with DHP; thereby, the interaction of fluoride and acetate may be reduced. Since water is highly polar and protic solvent, it can form hydrogen bond, therefore, the effect of cyanide on DHP was studied in different fractions of acetonitrile and water (Fig. 8A). The fluorescence in presence of cyanide is highest in 9:1 acetonitrile–water mixture. Under UV illumination in 9:1 acetonitrile–water mixture, a distinct turn-on changes from blue to cyan were observed only in presence of cyanide addition, not in presence of F^- or OAc^- (Fig. 8B). Other ions also did not produce any visual change in the emission (Fig. S6A). Thus, selective cyanide sensing can be achieved in 9:1 acetonitrile–-water mixture. Upon addition of cyanide ion, a new band was observed at about 395 nm in the absorption spectrum of DHP and the bands absorbance increases with cyanide concentration (Fig. 9). Though the

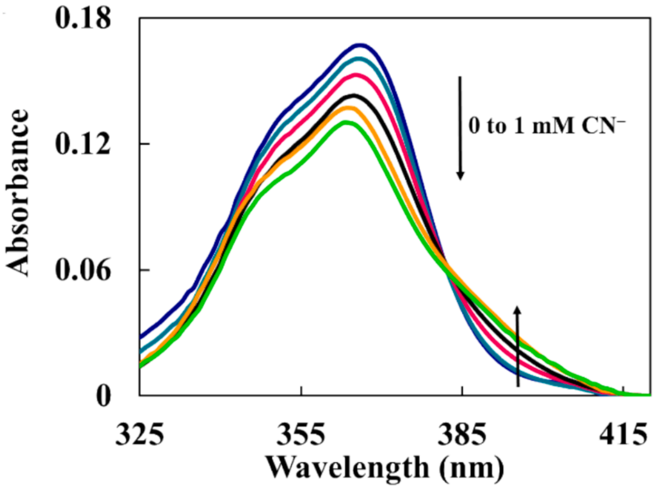

Fig. 9. Absorption spectra of DHP in presence of added CN^- (0–1 mM) in 9:1 acetonitrile: water mixture.

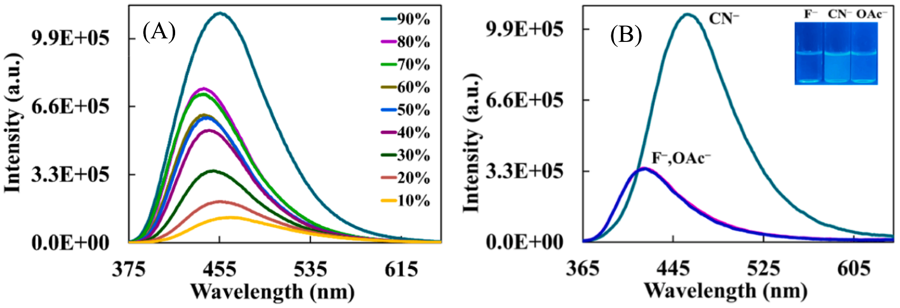

Fig. 8. Emission spectra of DHP (A) in presence of 1 mM CN^- varying acetonitrile and water percentage and (B) in presence of CN^-, F^- and OAc^- (1 mM) in 9:1 acetonitrile: water mixture.

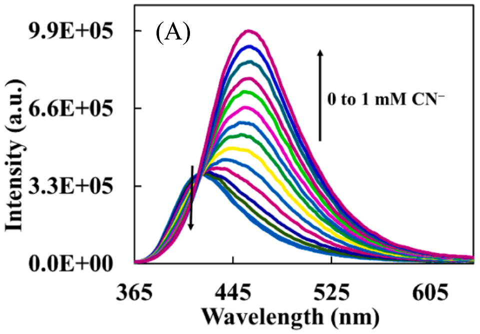

Fig. 10. Emission spectra of DHP (A) at $\lambda_{exc} = 350$ nm and (B) at $\lambda_{exc} = 400$ nm in presence of CN^- (0–1 mM) in 9:1 acetonitrile: water mixture.

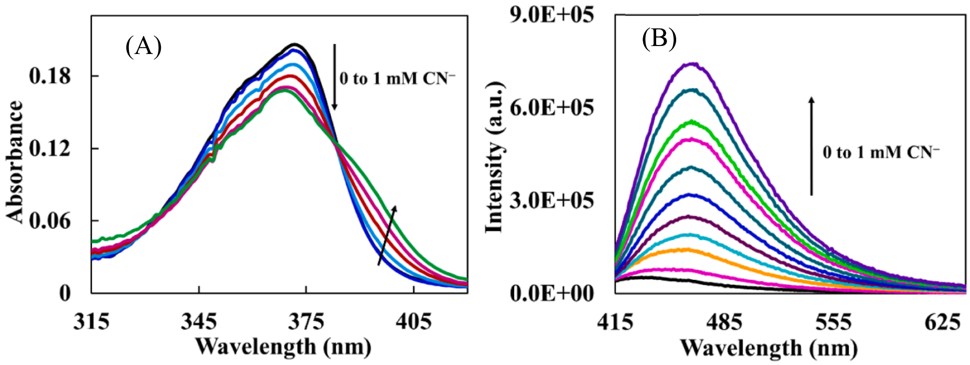

Fig. 11. (A) Absorption spectra and (B) emission spectra ($\lambda_{exc} = 400$ nm) of DHP in water 1 mM of CTAB solution with increasing concentration of CN^- (0–1 mM).

Table 2
Test Results for Evaluating CN^- levels in water samples.

Water samples	Added CN^- (μM)	Found CN^- (μM)	Accuracy (%)	RSD (%)
Deionised water	12	12.0	100	1.69
	20	20.0	100	1.74
Tap water	12	9.0	75	2.88
	20	17.4	87	0.88
River water	12	10.4	87	2.49
	20	18.7	93	2.13

Accuracy % = (detected cyanide concentration/added cyanide concentration) * 100.
Relative standard deviation (RSD) % = (standard deviation/mean) * 100.

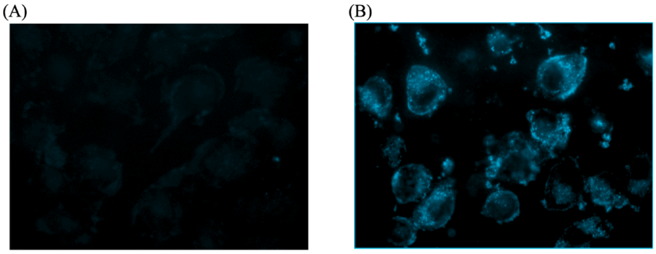

Fig. 12. Fluorescence imaging of MDA-MB 231 cells treated with (A) DHP and (B) DHP-CN^-.

absorbance of absorption band at ~365 nm is higher than that of ~395 nm band, its' absorbance decreased with addition of CN^-. The observation of 395 nm absorption band suggests the formation of anion in the ground state. This shows that in water in addition to DHP-CN^- complex, some amount of anion was also formed in the ground state. The emission spectra were recorded by exciting at 350 nm and 400 nm, excitation at both the wavelengths led to the formation of anion and the anionic emission was detected (Fig. 10(A and B)). In presence of 1 mM of CN^- an increment of ~10 times was triggered when excited with 400 nm light (Fig. 10B). The detection limit for CN^- in 9:1 acetonitrile: water mixture is 0.7 μM (Fig. S6B).

The impact of surfactant on DHP's sensing capability in the presence of 1 mM of CTAB solution was studied. Like in acetonitrile: water 9:1 mixture, in CTAB solution also with addition of CN^-, the band at ~370 nm decreases, along with appearance of anion band at 395 nm (Fig. 11A). In CTAB solution, the emission enhancement was 13 times in presence of 1 mM of CN^- (Fig. 11B) compared to 10 times in the presence of same concentration of cyanide ion in 9:1 acetonitrile: water mixtures. The LOD also improved to 0.2 μM in CTAB medium (Fig. S7).

3.3. *Real sample analysis, imaging and molecular logic gate*

Actual water samples may contain other ions, which may affect the detection of CN^-. For practical usage, water samples from Brahmaputra river, tap water from Amingaon (North Guwahati, Assam, India) were collected and filtered through a membrane with a pore size of 0.2 μm for further analysis. Different concentrations of cyanide,$^-$ 12 μM and 20 μM were added and recorded. Fluorescence titration curve with deionised water was considered as the standard, followed by the comparison of fluorescence signal of added cyanide to other water samples to calculate the actual CN^- levels (Table 2). Each experiment was repeated three times to calculate the relative standard deviation (RSD) with 75–93 % accuracy, justifying the applicability in real samples. Test paper strips were also prepared by immersing (1 cm × 3 cm) Whatman filter paper in probe DHP solution and then in CN^- solution (Fig. S8).

DHP has been further tested for tracking CN^- level in cellular environment in live cells. The presence of CN^- was detected in MDA-MB-231

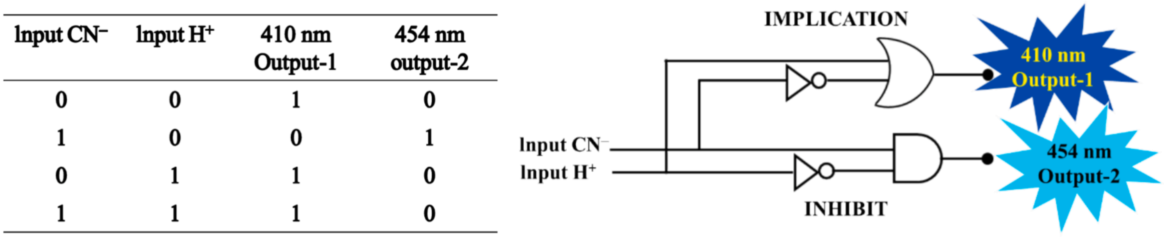

Input CN⁻	Input H⁺	410 nm Output-1	454 nm output-2
0	0	1	0
1	0	0	1
0	1	1	0
1	1	1	0

Fig. 13. Truth table and logic circuit of DHP with input CN⁻ and H⁺ (TFA) in acetonitrile.

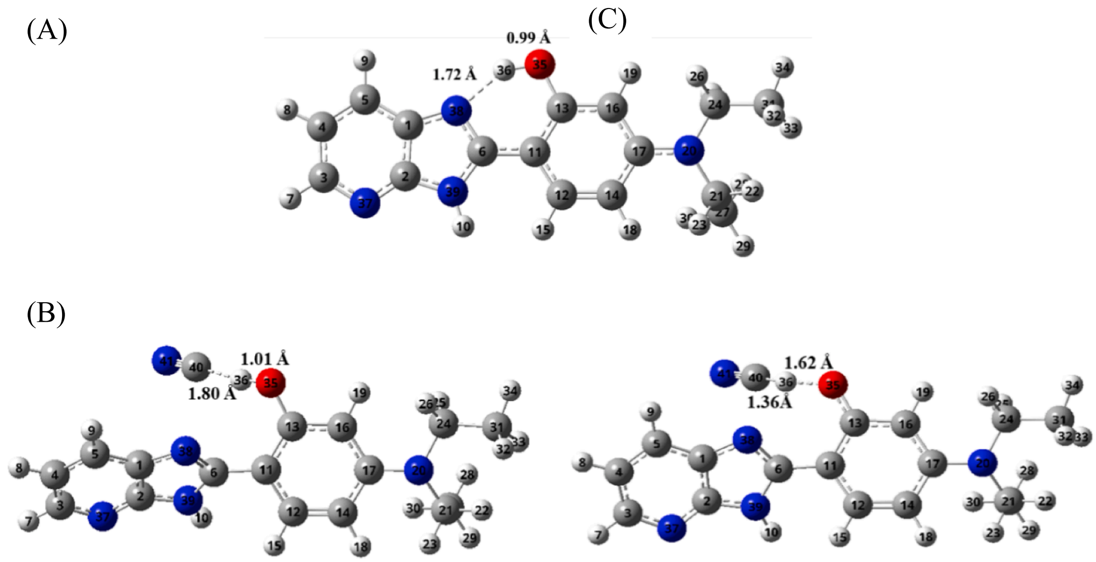

Fig. 14. Optimized structure of (A) DHP, (B) DHP-CN⁻ and (C) DHP⁻–HCN in ground state.

Table 3
Relative energy (eV with respect to ground state DHP-CN⁻), calculated and experimental electronic transition energies i.e. excitation and emission energies (eV), bond lengths (Å) for DHP and DHP-complexes in acetonitrile.

	DHP (Cis-enol)	DHP-CN⁻	DHP⁻–HCN
S_0 state			
Relative Energy		0.00	0.134
Distance			
N38 – H36	1.72	2.78	2.72
O35 – H36	0.99	1.01	1.62
C40 – H36	–	1.80	1.13
Excitation Energy[a]	3.43 (3.37)	3.54 (3.44)	3.13 (3.17)
S_1 state			
Relative Energy		3.218	3.004
Distance			
N38 – H36	1.70	2.61	2.55
O35 – H36	0.99	1.02	1.80
C40 – H36	–	1.76	1.09
Emission Energy[a]	3.04 (3.02)	3.03	2.72 (2.73)

[a] Value in parenthesis are experimental values.

cells by fluorescence microscopy imaging. The MDA-MB-231 breast cancer cells grown on cover slips were treated with CN– and their intracellular uptake was detected by the addition of DHP (3 μM). No fluorescence was observed in the absence of CN⁻ (Fig. 12A) whereas DHP produced bright fluorescence in the presence of CN⁻ (50 μM) (Fig. 12B). The fluorescence was observed in the cytoplasm of the cells suggesting that DHP can enter the live cells and can be used to track the presence of CN⁻ in the live cells by imaging. This opens up novel applications of DHP in tracking the presence of CN⁻ in biological tissues and cells.

Truth table and molecular logic circuit were constructed considering addition of CN⁻, H⁺ as chemical inputs and emission value 454 nm and 410 nm as output signals (Fig. 13). The inputs “0" and “1” specifies absence and presence of respective input signals and the output “1” and “0” suggests ON (fluorescence) and OFF (no fluorescence) state respectively.

3.4. *Theoretical approach to the mechanism of sensing*

To substantiate the mechanism of sensing, structures of DHP in cis-enol form, DHP-CN⁻ and DHP⁻–HCN were optimized in ground state (Fig. 14). Details of the optimized structures are provided in Table 3. The optimized structure of DHP indicates that the proton donor unit (O35 – H36) is intramolecular hydrogen bonded to the proton acceptor unit in the ground state, N38 – H36 hydrogen bond is 1.72 Å. Addition of cyanide broke the intramolecular hydrogen bond N38 – H36 (2.78 Å) by forming intermolecular hydrogen bond with C40 – H36 (1.80 Å) to form a more stable DHP-CN⁻ complex (Fig. 14B) The excitation energy calculated for DHP is 3.43 eV and for DHP-CN⁻ is 3.54 eV, which substantiates the observed blue shift in the absorption spectra with addition of CN⁻. The intermolecular proton transfer (H36) from DHP of oxygen to carbon (C40) atom of CN⁻ in DHP-CN⁻ results in DHP⁻–HCN (Fig. 14C). The O35 – H36 distance increases from 1.01 Å in DHP-CN⁻ to 1.62 Å in DHP⁻–HCN and C40 – H36 distance decreases from 1.80 Å in DHP-CN⁻ to 1.13 Å in DHP⁻–HCN complex. The calculated excitation energies of DHP, DHP-CN⁻, DHP⁻–HCN are also close to the experimental values, which confirms the assignment of DHP-CN⁻ and DHP⁻–HCN. However,

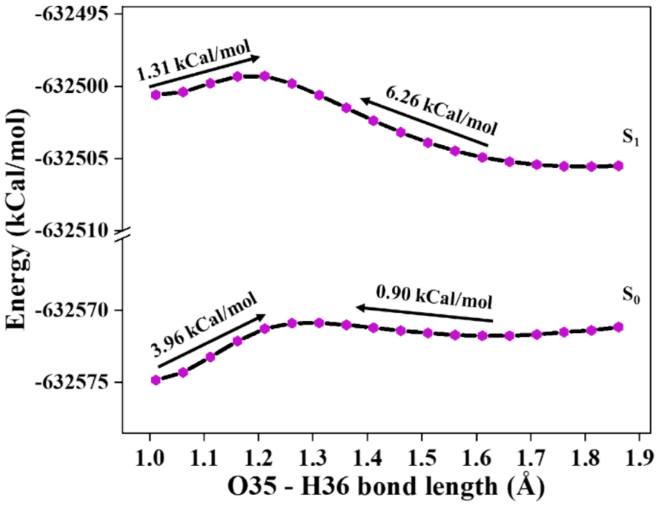

Fig. 15. PEC for DHP-CN$^-$ for S_0 and S_1 state varying O35 – H36 bond distance in acetonitrile.

the relative energy of DHP$^-$–HCN is higher than DHP-CN$^-$ in the ground state, therefore, the complex exists predominantly as DHP-CN$^-$ (where DHP is in neutral form) not as DHP$^-$–HCN (where DHP is in anionic form). The emission energy calculated for DHP-CN$^-$ and DHP$^-$–HCN, in comparison with experimental results, suggests the emission corresponds to DHP$^-$–HCN where DHP is in anionic form and not to DHP-CN$^-$ (Table 3). This further confirms the assignment of the emission of DHP in presence of cyanide ion to anionic emission. PEC in the ground and excited states were constructed (Fig. 15).

In the ground state, DHP-CN$^-$ is more stable than DHP$^-$–HCN by 0.134 eV, i.e., 3.08 kCal/mol (Fig. 15 and Fig. S9, Supplementary Materials). Additionally, from transition state (TS) structure, with a high negative frequency, was obtained through TSQ2 method. The barriers for the forward and reverse reactions are 3.98 kCal/mol and 0.90 kCal/mol, respectively (Fig. 15). These results are consistent with the experimental observation that the ground state equilibrium is dominated by DHP-CN$^-$ i.e., the DHP is in neutral form and forms intermolecular hydrogen bond with CN$^-$. However, in the excited state, its relative energy is higher than that of DHP$^-$–HCN. DHP$^-$–HCN is more stable than DHP-CN$^-$ by 0.214 eV i.e., 4.93 kCal/mol. The relative stability of DHP$^-$–HCN over DHP-CN$^-$ in the excited state is more than 1.5 times the relative stability of DHP-CN$^-$ over DHP$^-$–HCN in the ground state. Therefore, though DHP-CN$^-$ is the predominant complex in the ground

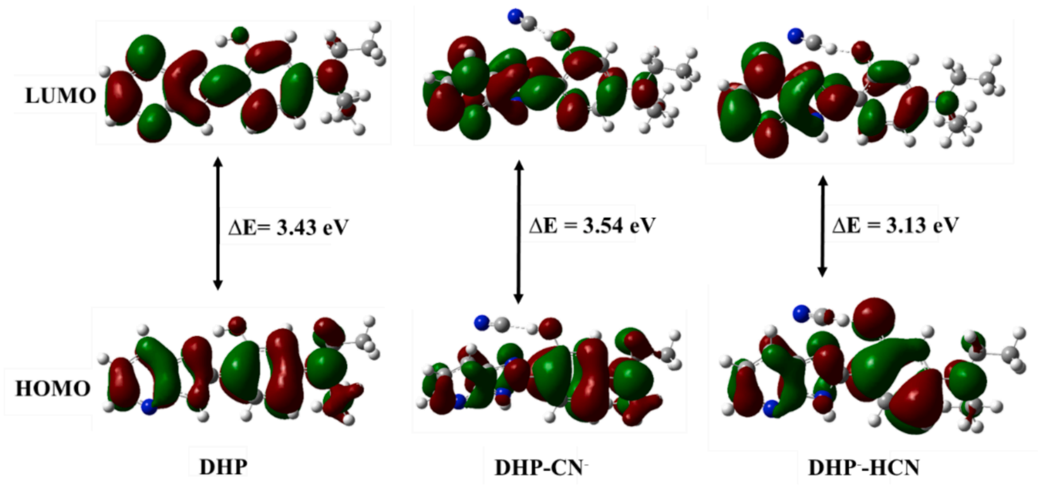

Fig. 16. Frontier molecular orbitals for S_0 to S_1 transition for DHP, DHP-CN$^-$ and DHP$^-$–HCN in acetonitrile.

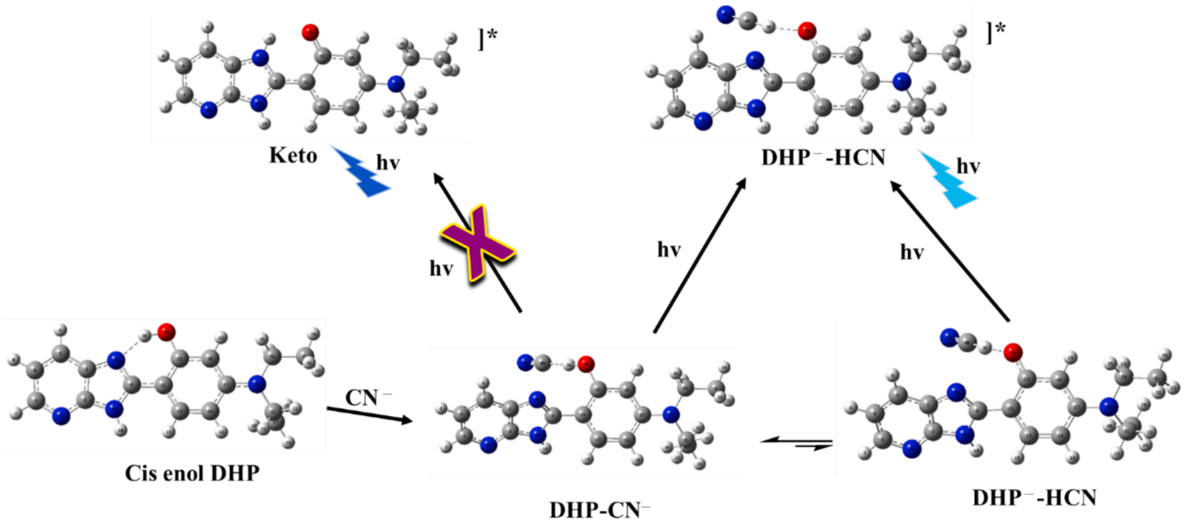

Scheme 1. The mechanism of cyanide ion sensing by DHP.

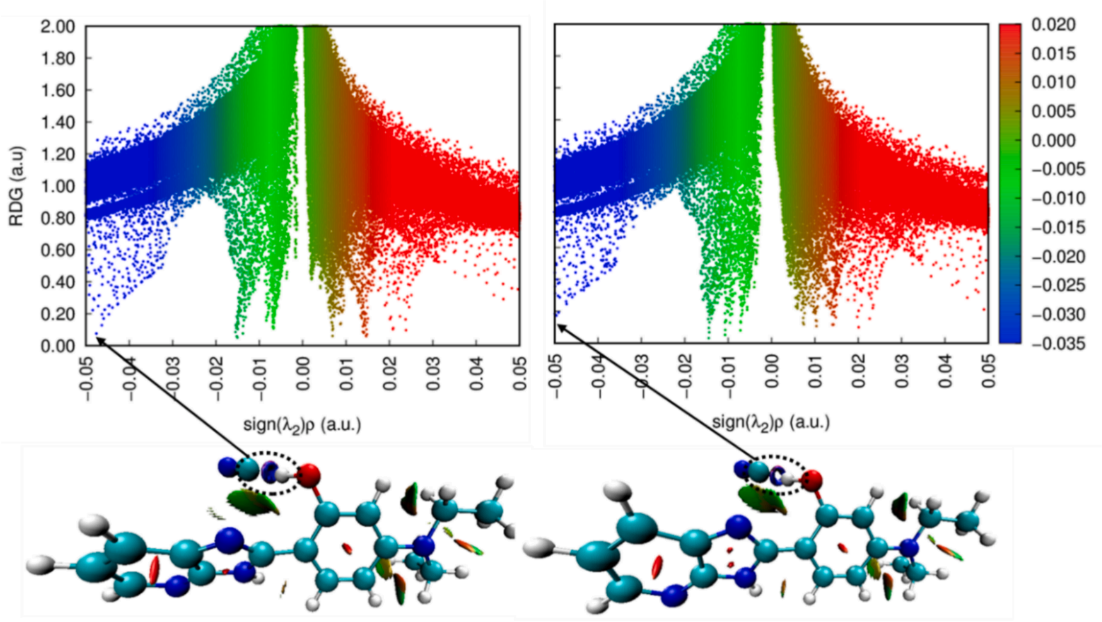

S_0 DHP-CN⁻ **S_1 DHP-CN⁻**

Fig. 17. The RDG scatter plots and the corresponding NCI isosurfaces assignments of each spike for DHP-CN⁻ in S_0 and S_1 states.

state, it exclusively undergoes intermolecular proton transfer to form DHP⁻–HCN in the excited state.

The Frontier molecular orbitals in S_0 to S_1 electronic transition are presented in Fig. 16. The electron density is distributed throughout the acceptor unit in all the structures and is very less around the donor diethyl amino group in particular in the excited state than in the ground state. Also, the anion formation is evident from the electron distribution in DHP⁻–HCN, where the electron density is more on the oxygen atom compared to the neutral DHP in the case of DHP-CN⁻.

The mechanism for cyanide sensing by DHP is presented in Scheme 1. As shown, upon addition of cyanide, it breaks the intramolecular hydrogen bond and forms DHP-CN⁻ complex. The intermolecular proton transfer results in anion formation, i.e. DHP⁻–HCN. The intermolecular proton transfer that led to anion formation is negligible in acetonitrile and increases in water and CTAB solutions. However, in all the solutions the anion formation is less in the ground state and DHP-CN⁻ complex is the predominant form where the fluorophore, neutral DHP has the intermolecular hydrogen bond through its ‘O–H’ hydrogen with CN⁻ i.e. DHP-CN⁻. However, excitation of both DHP⁻–HCN and DHP-CN⁻ results in anion emission. Upon excitation, the acidity of the ‘O–H’ is increased and due to the absence of an intramolecular hydrogen bond, ESIPT is averted and the intermolecular proton transfer occurs

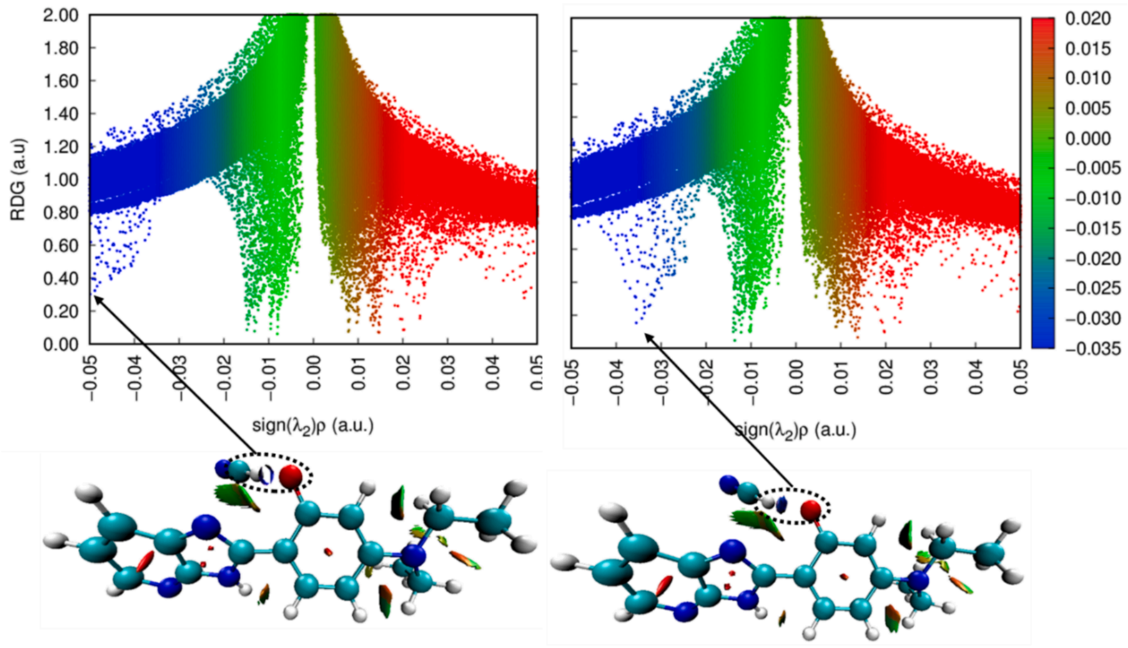

S_0 DHP⁻-HCN **S_1 DHP⁻-HCN**

Fig. 18. The RDG scatter plots and the corresponding NCI isosurfaces assignments of each spike for DHP⁻–HCN in S_0 and S_1 states.

through the intermolecular hydrogen bond. The calculation also revealed that the charge on the DHP oxygen decreased from −0.422 in the ground state to −0.402 in the first excited state in the DHP-CN^- complex (Fig. S10). On the other hand, the charge on the cyanide carbon in the same complex increased from −0.400 in the ground state to −0.412 in the first excited state. Thus, excitation of DHP in presence of cyanide ion results in anion emission.

Reduced density gradient (RDG) scatter plots visualize weak interactions, where blue, green and red colours represent hydrogen bond interactions, van der Waals interactions and steric repulsion, respectively. A high negative sign(λ2)ρ value signifies strong hydrogen bonding interaction, a high positive sign(λ2)ρ value signifies strong repulsive interaction and a closer to zero value indicates weak van der Waals interactions [56]. The scatter plot along with isosurface (Fig. S11) of DHP depicts stronger intramolecular hydrogen bond between –OH proton and −N= unit of fluorophore in the excited state (sign(λ2)ρ > −0.05) compared to the ground state (sign(λ2)ρ ~ −0.05). This suggests the stronger interaction between "N" and "H" in the excited state which initiates proton transfer from the proton donor to the acceptor in the excited state, which is evident from our previous reports [43]. Similarly, in DHP-CN^- hydrogen bond between –OH proton and carbon of CN^- is stronger in the excited state (sign(λ2)ρ > −0.05) than in the ground state (sign(λ2)ρ ~ −0.047) making –OH proton acidic in the excited state which promotes intermolecular proton transfer toward carbon atom of CN^- (Fig. 17). On the contrary, in DHP^-–HCN, the hydrogen bond between oxygen atom and proton of HCN is weaker in the excited state ((sign(λ2)ρ ~ −0.035) than in the ground state (sign(λ2)ρ > −0.05) (Fig. 18). Therefore, upon excitation, the intermolecular proton transfer from DHP to CN^- is favoured and the reverse intermolecular proton transfer i.e. from HCN to DHP^- is unfavoured.

The sensing performance of DHP was compared with some of the reported sensors [6,13,20,21,38,41,57,58] (Table S1, Supplementary Material].

4. Conclusions

DHP acts as a turn on fluorescence sensor for cyanide sensing with LOD of 0.02 μM in acetonitrile. However, fluoride ions and acetate ions also turn on the cyan fluorescence. DHP can be tuned to sense only cyanide ion in 9:1 acetonitrile aqueous mixture and it has LOD of 0.7 μM. The LOD can be improved to 0.2 μM by using cationic micelle CTAB. The mechanism for detection of cyanide in organic and aqueous solutions is by fluorescence turn-on effect due to anion formation. Addition of cyanide results in the formation of complex between the fluorophore and cyanide ion. Upon excitation, the DHP-CN^- complex undergoes intermolecular proton transfer that produces DHP anion, that has cyan colour strong fluorescence. It can be reversibly protonated with TFA to give back the original emission of DHP. DFT calculations also suggested that in the ground state, the fluorophore predominantly exists in neutral form, forming a complex with cyanide ion. It further suggested that in presence of CN^-, the anionic form of DHP is energetically favoured over the neutral form in the excited state. The transition state calculation and RDG scatter plots also support the mechanism of intermolecular proton transfer associated with anion formation, which corroborates well with experimental findings. The response is utilised in the construction of molecular logic gates and for the detection and imaging of CN^- in MDA-MB-231 breast cancer cells. Further, the fluorophore was tested in different water samples which showed accuracy of 75–93 %.

CRediT authorship contribution statement

Mongoli Brahma: Investigation, Methodology, Validation, Formal analysis, Data curation, Writing – original draft, Visualization. **Arup Das Kanungo:** Methodology, Formal analysis. **Minati Das:** Formal analysis. **Sam P. Mathew:** Investigation. **Bithiah Grace Jaganathan:** Formal analysis, Writing – review & editing. **G. Krishnamoorthy:** Conceptualization, Investigation, Formal analysis, Writing – review & editing, Visualization, Supervision, Project administration, Funding acquisition.

Declaration of competing interest

The authors declare that they have no known competing financial interests or personal relationships that could have appeared to influence the work reported in this paper.

Acknowledgements

The article is dedicated to Prof. S. K. Dogra on his 83rd Birthday. The authors thank Central Instruments Facility, IIT Guwahati for Life-Spec-II instrument for decay measurement. We also acknowledge PARAM-ISHAN supercomputing Facility, Computer and Communication Center, IIT Guwahati for high performance computing facility. The authors also acknowledge Department of Biotechnology (DBT), India for the financial support for the project no. BT/NER/143/SP44675/2023.

Appendix A. Supplementary data

Supplementary data includes NMR Spectra, Mass spectrum, Job plot, Benesi-Hildebrand plot, LOD plots, Fluorescence image under UV illumination, Paper strip images, TS energy level diagram, Mulliken charges images, RDG scatter plots, Comparison table for different cyanide sensors, Coordinates of optimized geometries. Supplementary data to this article can be found online at https://doi.org/10.1016/j.saa.2025.126203.

Data availability

No data was used for the research described in the article.

References

[1] C. Young, L. Twidwell, C. Anderson, Cyanide: social, industrial, and economic aspects, Minerals, Metals and Materials Society, Warrendale, 2001.
[2] D.T. Thompson, Cyanide: Social, industrial and economic aspects, Gold Bull. 34 (2001) 133, https://doi.org/10.1007/bf03214826.
[3] M. Tahir Waseem, H. Muhammad Junaid, S. Majeed, A. Muhammad Khan, T. Mahmood, S. Anjum Shahzad, Fluorene based fluorescent and colorimetric chemosensors for selective detection of cyanide ions in aqueous medium and application of logic gate, Microchem. J. 173 (2022) 107018, https://doi.org/10.1016/j.microc.2021.107018.
[4] E.M. Ramzy, Toxicity and stability of sodium cyanide in fresh water fish Nile tilapia, Water Sci. 28 (2014) 42–50, https://doi.org/10.1016/j.wsj.2014.09.002.
[5] D. Aydin, Sensing of aluminum and cyanide ions utilizing a novel bis-phenol a based fluorogenic probe: Applications in test stripts, Microchem. J. 159 (2020) 105477, https://doi.org/10.1016/j.microc.2020.105477.
[6] R. Bhaskara, V. Vijayakumar, V. Srinivasadesikan, S.-L. Lee, S. Sarveswari, Rationally designed imidazole derivative as colorimetric and fluorometric sensor for selective, qualitative and quantitative cyanide ion detection in real time samples, Spectrochim. Acta A Mol. Biomol. Spectrosc. 234 (2020) 118212, https://doi.org/10.1016/j.saa.2020.118212.
[7] T.C. Marrs, R.L. Maynard, F.R. Sidell, Chemical warfare agents: Toxicology and treatment, (2007). doi: 10.1002/9780470060032.
[8] H. Li, T. Chen, L. Jin, Y. Kan, B. Yin, Colorimetric and fluorometric dual-modal probes for cyanide detection based on the doubly activated Michael acceptor and their bioimaging applications, Anal. Chim. Acta 852 (2014) 203–211, https://doi.org/10.1016/j.aca.2014.09.018.
[9] F. Moriya, Y. Hashimoto, Potential for error when assessing blood cyanide concentrations in fire victims, J. Forensic Sci. 46 (2001) 1421–1425, https://doi.org/10.1520/jfs15165j.
[10] World Health Organization, Guidelines for Drinking-Water Quality: Recommendations. World Health Organization, 2004.
[11] L. Wang, Y. Gan, X. Ran, D. Cao, Simultaneous sensing cyanide and fluoride by Lewis acidic atom regulated–chromophore reaction and applications in real samples, Microchem. J. 207 (2024) 111832, https://doi.org/10.1016/j.microc.2024.111832.
[12] S. Uotaa, B.-J. Hwange, R. Butcherb, R. Mullins, J. Wachirac, Y. Hijjia, F. Abebe, A simple benzothiazolium-based sensor for cyanide detection: Applications in environmental analysis and bioimaging, Spectrochim. Acta A Mol. Biomol. Spectrosc. 326 (2025) 125155, https://doi.org/10.1016/j.saa.2024.125155.

[13] C. Rao, Z. Wang, Z. Li, L. Chen, C. Fu, T. Zhu, X. Chen, Z. Wang, C. Liu, Pyridine-hydrazone-controlled cyanide detection in aqueous media and solid-state: tuning the excited-state intramolecular proton transfer (ESIPT) fluorescence modulated by intramolecular NH⋯Br hydrogen bonding, Analyst 145 (2020) 1062–1068, https://doi.org/10.1039/c9an01762c.

[14] L. Wu, H. Xu, M. Shen, Y. Li, Q. Yang, Y. Li, An innovative fluorescent probe for the detection of cyanide - enhanced sensitivity by controlling its electrostatic potential and suitable for applications such as cell imaging and food analysis, Spectrochim. Acta A Mol. Biomol. Spectrosc. 305 (2024) 123443, https://doi.org/10.1016/j.saa.2023.123443.

[15] Z. Xu, X. Chen, H.N. Kim, J. Yoon, Sensors for the optical detection of cyanide ion, Chem. Soc. Rev. 39 (2010) 127–137, https://doi.org/10.1039/b907368j.

[16] S.D. Padghan, J.-W. Hu, Y.-H. Hsu, K.-M. Liu, K.-Y. Chen, Swift and quantitative naked-eye detection of cyanide: A dual-mode approach using an ICT-based colorimetric and ratiometric fluorescent chemodosimeter, Dyes Pigm. 228 (2024) 112229, https://doi.org/10.1016/j.dyepig.2024.112229.

[17] C.I. David, J. Lee, K. Ramanagul, V. Gothandapani, B.J. Kim, H.-l Lee, Dual channel chemosensor for successive detection of environmentally toxic Pd^{2+} and CN^{-} ions and its application to cancer cell imaging, Anal. Chim. Acta 1305 (2024) 342582, https://doi.org/10.1016/j.aca.2024.342582.

[18] S. Majeed, M.T. Waseem, H.M. Junaid, G.S. Khan, S. Nawazish, T. Mahmood, A. M. Khan, S.A. Shahzad, Aggregation induced emission based fluorenes as dual-channel fluorescent probes for rapid detection of cyanide: applications of smartphones and logic gates, RSC Adv. 12 (2022) 18897–18910, https://doi.org/10.1039/d2ra03119a.

[19] C. Das, A. Mondal, S. Sengupta, C. Cardin, S.K. Chattopadhyay, Selective cyanide sensing using a Fe(III) complex of pyridoxal-beta alanine Schiff base, Spectrochim. Acta A Mol. Biomol. Spectrosc. 273 (2022) 120943, https://doi.org/10.1016/j.saa.2022.120943.

[20] F. Huo, Y. Zhang, Y. Yue, J. Chao, Y. Zhang, C. Yin, Isophorone-based aldehyde for “ratiometric” detection of cyanide by hampering ESIPT, Dyes Pigm. 143 (2017) 270–275, https://doi.org/10.1016/j.dyepig.2017.04.050.

[21] T. Zhu, Y. Hu, X. Chen, H. Shao, Z. Chen, H. Zhang, C. Liu, Novel chromene-derived fluorescent probe for detection of cyanides by imine-controlled ESIPT, Dyes Pigm. 195 (2021) 109693, https://doi.org/10.1016/j.dyepig.2021.109693.

[22] S. Goswami, A. Manna, S. Paul, A.K. Das, K. Aich, P.K. Nandi, Resonance-assisted hydrogen bonding induced nucleophilic addition to hamper ESIPT: ratiometric detection of cyanide in aqueous media, Chem. Commun. (Camb) 49 (2013) 2912–2914, https://doi.org/10.1039/c3cc39256b.

[23] S. Goswami, A. Manna, S. Paul, K. Aich, A.K. Das, S. Chakraborty, Highly reactive (<1 min) ratiometric probe for selective ‘naked-eye’ detection of cyanide in aqueous media, Tetrahedron Lett. 54 (2013) 1785–1789, https://doi.org/10.1016/j.tetlet.2012.12.092.

[24] S.D. Padghan, L.-C. Wang, W.-C. Lin, J.-W. Hu, W.-C. Liu, K.-Y. Chen, Rational design of an ICT-based chemodosimeter with aggregation-induced emission for colorimetric and ratiometric fluorescent detection of cyanide in a wide pH range, ACS Omega 6 (2021) 5287–5296, https://doi.org/10.1021/acsomega.0c05409.

[25] N. Tohora, M. Mahato, T. Sultana, S. Ahamed, S. Ghanta, S.K. Das, A benzoxazole-based fluorescent ‘off-on-off’ probe for cascade recognition of cyanide and Fe^{3+} ions, J. Photochem. Photobiol. A Chem. 442 (2023) 114807, https://doi.org/10.1016/j.jphotochem.2023.114807.

[26] V. Yadav, V.K. Bhardwaj, Tuning the sensing properties of isophthalic dihydrazide-based receptor via formation of organic–inorganic hybrid and metal complex: An enhanced sensing activity for Hg2+ and CN− detection in semi-aqueous medium, Microchem. J. 202 (2024) 110739, https://doi.org/10.1016/j.microc.2024.110739.

[27] S.D. Padghan, J.-W. Hu, L.-C. Wang, F.-Y. Wang, K.-Y. Chen, Low-molecular-weight J-aggregate solid red emitter for selective and quantitative detection of cyanide, Chem. Asian J. 18 (2023), https://doi.org/10.1002/asia.202201293 e202201293.

[28] T. Cheng, T. Wang, W. Zhu, Y. Yang, B. Zeng, Y. Xu, X. Qian, Modulating the selectivity of near-IR fluorescent probes toward various metal ions by judicious choice of aqueous buffer solutions, Chem. Commun. (Camb.) 47 (2011) 3915–3917, https://doi.org/10.1039/c0cc05554a.

[29] O.A. Pegu, G. Das, Twisted-intramolecular-charge-transfer based fluorogenic nano-probes for ultrafast cyanide sensing in water and micellar medium, J. Mater. Chem. C Mater. Opt. Electron. Devices 12 (2024) 6519–6527, https://doi.org/10.1039/d4tc00643g.

[30] N. Kumari, N. Dey, S. Jha, S. Bhattacharya, Ratiometric, reversible, and parts per billion level detection of multiple toxic transition metal ions using a single probe in micellar media, ACS Appl. Mater. Interfaces 5 (2013) 2438–2445, https://doi.org/10.1021/am400063k.

[31] G. Sun, W. Chen, Y. Liu, X. Jin, Z. Zhang, J. Su, A novel colorimetric and fluorometric probe for the detection of CN^{-} with high selectivity in aqueous media, Dyes Pigm. 176 (2020) 108224, https://doi.org/10.1016/j.dyepig.2020.108224.

[32] Y. Zhang, D. Li, Y. Li, J. Yu, Solvatochromic AIE luminogens as supersensitive water detectors in organic solvents and highly efficient cyanide chemosensors in water, Chem. Sci. 5 (2014) 2710–2716, https://doi.org/10.1039/C4SC00721B.

[33] Kiran, A. Ranolia, Priyanka, I. Bala, J. Jangir, S. Singh, J. Sindhu, P. Kumar, D. Singh, Rationally designed dual channel reversible probe for cyanide recognition in aqueous medium with solid-state sensing abilities, J. Photochem. Photobiol. A Chem. 453 (2024) 115650, https://doi.org/10.1016/j.jphotochem.2024.115650.

[34] T. Xie, Y. Li, M. Zhang, L. Wang, Y. Hu, K. Yin, S. Fan, H. Wu, Aggregation-induced emission activity of sensor TBM-C1 hybrid of methoxy-triphenylamine (OMe-TPA) and dicyanovinyl for cyanide detection in aqueous THF: Mechanistic insights and potential applications, Spectrochim. Acta A Mol. Biomol. Spectrosc. 312 (2024) 124058, https://doi.org/10.1016/j.saa.2024.124058.

[35] L. Li, M. Zan, X. Qie, P. Miao, J. Yue, Z. Chang, Z. Wang, F.-Q. Bai, H.-X. Zhang, J. K. Ferri, W.-F. Dong, A highly selective fluorescent probe for cyanide ion and its detection mechanism from theoretical calculations, Talanta 185 (2018) 1–6, https://doi.org/10.1016/j.talanta.2018.03.013.

[36] P.Q. Nhien, W.-L. Chou, T.T.K. Cuc, T.M. Khang, C.-H. Wu, N. Thirumalaivasan, B. T.B. Hue, J.I. Wu, S.-P. Wu, H.-C. Lin, Multi-stimuli responsive FRET processes of bifluorophoric AIEgens in an amphiphilic copolymer and its application to cyanide detection in aqueous media, ACS Appl. Mater. Interfaces 12 (2020) 10959–10972, https://doi.org/10.1021/acsami.9b21970.

[37] R. Khalid, S.A. Shahzad, M.A. Assiri, T. Javid, H. Irshad, M.Z. Ullah, AIE active fluorescent probe for the detection of cyanide ion through fluorescence enhancement in real samples: An integrated extensive fluorescence and DFT studies, Microchem. J. 200 (2024) 110264, https://doi.org/10.1016/j.microc.2024.110264.

[38] C. Liang, S. Jiang, Fluorescence light-up detection of cyanide in water based on cyclization reaction followed by ESIPT and AIEE, Analyst 142 (2017) 4825, https://doi.org/10.1039/C7AN01479A.

[39] A. Pal, O. Sarkar, N.R. Pramanik, N. Dey, Design of ESIPT-based fluorescent probes for dual-mode sensing of cyanide: application to rapid on-location detection and screening of natural water samples, Ind. Eng. Chem. Res. 63 (2024) 8489–8496, https://doi.org/10.1021/acs.iecr.3c04209.

[40] Ila, M. Brahma, S. Ranjan, P. Tripathi, G. Krishnamoorthy, Modifying the proton transfer of 3,5-bis(2-hydroxyphenyl)-1H-1,2,4-triazole by water, confinement and confined water, Spectrochim. Acta A Mol. Biomol. Spectrosc. 272 (2022) 120911, https://doi.org/10.1016/j.saa.2022.120911.

[41] S.B. Roy, A. Maity, K.K. Rajak, A turn-off fluorescence sensor for cyanide detection which in turn inhibit 2-way ESIPT investigated by experimental and theoretical study, Inorg. Chem. Commun. 76 (2017) 81–86, https://doi.org/10.1016/j.inoche.2017.01.009.

[42] B.K. Bakht, H. Zali-Boeini, M. Torabi, M. Shams-Harandi, E. Shams, Z. Farahbakhsh, R.S. Varma, Optical, electrochemical, and test strip methods for sensitive and selective detection of Cyanide ion using a multifunctional π-extended azaacene-based system, Sens. Actuators B Chem. 379 (2023) 133280, https://doi.org/10.1016/j.snb.2022.133280.

[43] M. Das, M. Brahma, G. Krishnamoorthy, Light-driven switching between intramolecular proton-transfer and charge-transfer states, J. Phys. Chem. B 125 (2021) 2339–2350, https://doi.org/10.1021/acs.jpcb.0c09705.

[44] M.J. Frisch, G.W. Trucks, H.B. Schlegel, G.E. Scuseria, M.A. Robb, J.R. Cheeseman, G. Scalmani, V. Barone, G.A. Petersson, H. Nakatsuji, X. Li, M. Caricato, A.V. Marenich, J. Bloino, B.G. Janesko, R. Gomperts, B. Mennucci, H.P. Hratchian, J.V. Ortiz, A.F. Izmaylov, J.L. Sonnenberg, D. Williams-Young, F. Ding, F. Lipparini, F. Egidi, J. Goings, B. Peng, A. Petrone, T. Henderson, D. Ranasinghe, V.G. Zakrzewski, J. Gao, N. Rega, G. Zheng, W. Liang, M. Hada, M. Ehara, K. Toyota, R. Fukuda, J. Hasegawa, M. Ishida, T. Nakajima, Y. Honda, O. Kitao, H. Nakai, T. Vreven, K. Throssell, J.A. Montgomery, Jr., J.E. Peralta, F. Ogliaro, M.J. Bearpark, J.J. Heyd, E.N. Brothers, K.N. Kudin, V.N. Staroverov, T.A. Keith, R. Kobayashi, J. Normand, K. Raghavachari, A.P. Rendell, J.C. Burant, S.S. Iyengar, J. Tomasi, M. Cossi, J.M. Millam, M. Klene, C. Adamo, R. Cammi, J.W. Ochterski, R.L. Martin, K. Morokuma, O. Farkas, J.B. Foresman, D.J. Fox, Gaussian, Inc., Wallingford CT, 2016.

[45] R.D. Dennington, T.A. Keith, J.M. Millam, GaussView 5.0.8, Gaussian, 2008.

[46] A.D. Becke, Density-functional thermochemistry. III. The role of exact exchange, J. Chem. Phys. 98 (1993) 5648–5652, https://doi.org/10.1063/1.464913.

[47] C. Lee, W. Yang, R.G. Parr, Development of the colle-salvetti correlation-energy formula into a functional of the electron density, Phys. Rev. B Condens. Matter 37 (1988) 785–789, https://doi.org/10.1103/physrevb.37.785.

[48] J.-D. Chai, M.H. Gordon, Long-range corrected hybrid density functionals with damped atom-atom dispersion corrections, PCCP 10 (2008) 6615–6620, https://doi.org/10.1039/b810189b.

[49] A. Das Kanungo, Ila, S. Panda, U. Phukon, M. Sathiyendran, G. Krishnamoorthy, Excited state dynamics of a double ESIPT unit comprising fluorophore, J. Photochem. Photobiol. A Chem. 450 (2024) 115412, https://doi.org/10.1016/j.jphotochem.2023.115412.

[50] I. Deperasińska, D.T. Gryko, E. Karpiuk, B. Kozankiewicz, A. Makarewicz, J. Piechowska, 12-hydroxy-1-azaperylene—limiting case of the ESIPT system: Enol-keto tautomerization in S$_0$ and S$_1$ states, Chem. A Eur. J. 116 (2012) 2109–2116, https://doi.org/10.1021/jp2103353.

[51] J. Vial, A. Jardy, Experimental comparison of the different approaches to estimate LOD and LOQ of an HPLC method, Anal. Chem. 71 (1999) 2672–2677, https://doi.org/10.1021/ac981179n.

[52] H.A. Bensi, J.H. Hildebrand, A spectrophotometric investigation of the interaction of iodine with aromatic hydrocarbons, J. Am. Chem. Soc. 71 (1949) 2703–2707, https://doi.org/10.1021/ja01176a030.

[53] T. Lu, F. Chen, Multiwfn: a multifunctional wavefunction analyser, J. Comput. Chem. 33 (2012) 580–592, https://doi.org/10.1002/jcc.22885.

[54] W. Humphrey, A. Dalke, K. Schulten, VMD: visual molecular dynamics, J. Mol. Graph. Model. 14 (1996) 33–38, https://doi.org/10.1016/0263-7855(96)00018-5.

[55] M. Das, M. Brahma, G. Krishnamoorthy, Controlling the photoswitching of 2-(4′-diethylamino-2′-hydroxyphenyl)-1*H*-imidazo-[4,5-b]pyridine by pH, J. Photochem. Photobiol. A Chem. 421 (2021) 113504, https://doi.org/10.1016/j.jphotochem.2021.113504.

[56] Y. Wang, T. Bai, P. Song, Z. Tang, Z. Lou, New insight into the fluorescence mechanism in a fluorescent probe for detecting Zn^{2+} and CN^{-} through theoretical

calculations, J. Mol. Liq. 343 (2021) 117539, https://doi.org/10.1016/j.molliq.2021.117539.

[57] M.S. Kim, D. Yun, J.B. Chae, H. So, H. Lee, K.-T. Kim, M. Kim, M.H. Lim, C. Kim, A Novel Thiophene-Based Fluorescent Chemosensor for the Detection of Zn^{2+} and CN^- Imaging Applications in Live Cells and Zebrafish, Sensors 19 (2019) 5458, https://doi.org/10.3390/s19245458.

[58] L. Tang, L. Zhou, A. Liu, X. Yan, K. Zhong, X. Liu, X. Gao, J. Li, A new cascade reaction-based colorimetric and fluorescence "turn on" dual-function probe for cyanide and hydrazine detection, Dyes Pigm. 186 (2021) 109034, https://doi.org/10.1016/j.dyepig.2020.109034.